Numerical modeling of temperature and species distributions in hydrocarbon reservoirs

Edward W. Bolton[1] and Abbas Firoozabadi[2,3]

Received 12 January 2013; revised 22 October 2013; accepted 25 October 2013; published 8 January 2014.

[1] We examine bulk fluid motion and diffusion of multicomponent hydrocarbon species in porous media in the context of nonequilibrium thermodynamics, with particular focus on the phenomenology induced by horizontal thermal gradients at the upper and lower horizontal boundaries. The problem is formulated with respect to the barycentric (mass-averaged) frame of reference. Thermally induced convection, with fully time-dependent temperature distributions, can lead to nearly constant hydrocarbon composition, with minor unmixing due to thermal gradients near the horizontal boundaries. Alternately, the composition can be vertically segregated due to gravitational effects. Independent and essentially steady solutions have been found to depend on how the compositions are initialized in space and may have implications for reservoir history. We also examine injection (to represent filling) and extraction (to represent leakage) of hydrocarbons at independent points and find a large distortion of the gas-oil contact for low permeability.

Citation: Bolton, E. W., and A. Firoozabadi (2014), Numerical modeling of temperature and species distributions in hydrocarbon reservoirs, *J. Geophys. Res. Solid Earth*, *119*, 18–31, doi:10.1002/2013JB010043.

1. Introduction

[2] Thermal convection in porous media is relevant in many contexts of Earth sciences. In plane layers [*Caltagirone*, 1975] heated from below with constant temperature horizontal boundaries the critical Rayleigh number is $4\pi^2$ for constant porosity and permeability. Porous media thermal convection has also been studied in sloping layers [*Bories and Combarnous*, 1973] and with mineral dissolution and precipitation [*Wood and Hewett*, 1982; *Palm*, 1990; *Bolton et al.*, 1996, 1999]. Here we revisit the problem of thermal convection in porous media in the context of multicomponent hydrocarbon reservoirs in a horizontal layer. We used initial conditions with imposed horizontal and vertical temperature gradients. Simulations starting with these initial thermal conditions, the temperature in the computational domain can either be fixed or can be allowed to evolve in time by advection of heat with vanishing horizontal heat flux at the lateral boundaries.

[3] Compositional evolution of hydrocarbon reservoirs depends on fluid phase behavior, charging, leakage, reactions, diffusion of species, and bulk fluid motion. These processes all have different time scales leading to complex and variable behavior.

[1]Department of Geology and Geophysics, Yale University, New Haven, Connecticut, USA.

[2]Department of Chemical and Environmental Engineering, Yale University, New Haven, Connecticut, USA.

[3]Reservoir Engineering Research Institute, Palo Alto, California, USA.

Corresponding author: E. W. Bolton, Yale University, Department of Geology and Geophysics, Kline Geology Laboratory, P.O. Box 208109, New Haven, CT 06520-8109, USA. (edward.bolton@yale.edu)

2169-9313/14/10.1002/2013JB010043

[4] Previous studies of hydrocarbon compositional gradients have examined the influence of thermal, pressure, and molecular diffusion that leads to compositional variation due to fixed, but independent, thermal gradients in the horizontal and vertical directions [*Riley and Firoozabadi*, 1998; *Ghorayeb and Firoozabadi*, 2000b; *Ghorayeb et al.*, 2003; *Nasrabadi et al.*, 2007; *Abbasi et al.*, 2011]. Here we allow the temperature to evolve dynamically due to advection of heat. One surprising result of this research is that two independent steady states of the same average composition can occur depending on the initial conditions. In addition, uniform composition reservoirs can slightly "unmix" due to the diffusion induced by pressure and temperature gradients. Thermal convection, if vigorous enough, can keep compositions nearly uniform, although there are other contexts in which significant segregation can occur. Nearly constant composition oil fields are cited by *Ghorayeb and Firoozabadi* [2000a]. We suggest that the filling history or vigorous convection in high-permeability reservoirs could influence whether an oilfield is nearly uniform or highly stratified with respect to composition.

[5] Numerous factors influence the time scales over which a particular reservoir composition changes, including its size, temperature, permeability, porosity, and mean composition. Diffusion of petroleum components can occur due to gradients in temperature, pressure, and composition. Within a petroleum reservoir, the low molecular weight components tend to increase (in mole fraction) going upward, while the high molecular weight components tend to increase going downward, both due to gravity segregation. This often leads to a "gas cap" and a "gas-oil contact" (GOC) where a vapor phase lies above a liquid phase. The fact that hydrocarbon reservoirs can have compositions that are vertically segregated due to gravitational effects is similar to the

compositional changes in the vertical in the atmosphere [*Chapman*, 1955]. In addition to diffusive fluxes, the fluids can advect due to density gradients arising from compositional or thermal gradients in the horizontal. Buoyancy driven flow can also modify the thermal structure of the reservoir by advection of heat. In the oil field lifetime, compositions can also vary due to charging or leakage from one zone to another. Matrix porosity, permeability, and tortuosity, and the heterogeneous and anisotropic (of the latter two) distribution of these can have a profound influence upon how fluids move through the reservoir. Over the long term, reactions and filling / leakage history can also modify the oilfield compositions [*Helgeson et al.*, 2009; *Leythaeuser and Rückheim*, 1989; *di Primio and Skeie*, 2004]. In addition, petroleum fluids can displace saline water. The matrix itself can evolve due to compaction and fracturing. Here, we do not consider reactive maturation or the evolution of the solid matrix.

[6] Compositional variations in time and space are important for understanding the evolution of oilfields. Measurements of compositions, pressures, and temperatures in various places in a reservoir can suggest whether various zones within the domain are connected or isolated. Closed reservoirs should approach predictable compositional variations. The influence of temperature and pressure gradients, along with porosities and permeabilities, can provide the knowledge whether steady states should be expected or whether the system may still be evolving compositionally. It should be emphasized that compositional and thermal evolution of confined reservoirs can exhibit a large variety of time dependencies. Although our emphasis in this paper is on systems that evolve to nearly steady states, greater thermal forcing or higher permeability can result in unsteady and/or chaotic thermal convection with compositions continuously evolving.

[7] We simulate the evolution of the composition of petroleum reservoirs in two-dimensional domains using the finite volume approach. Diffusive fluxes due to gradients in pressure, temperature, and composition are calculated, as well as convection due to buoyancy. The Peng-Robinson equation of state is used to calculate fluid properties and phase stability as necessary in conjunction with phase split (flash) calculations [*Firoozabadi*, 1999]. Any location has the potential of having one or two stable phases. Anisotropic permeability and specified rates of injection and leakage at different locations are allowed. Nonideal multicomponent molecular diffusion coefficients have been adopted from *Leahy-Dios and Firoozabadi* [2007].

[8] The thermal structure can be assigned or allowed to evolve. Two distinct initial conditions for the fluid composition are allowed. One choice is "uniform composition" and pressure throughout the domain (CCI: constant composition initialization). In this case, the pressure quickly adjusts to be near hydrostatic, and the other diffusive and advective processes allow continuous compositional evolution. As the fluid is not stratified with respect to composition, fluid motion in the vertical direction arising from thermal convection is not inhibited.

[9] The other choice for initial fluid composition is to solve for the composition that would have diffusion fluxes vanish in the vertical direction. This is called the "convection-free initialization" (CFI) [*Nasrabadi et al.*, 2006]. The thermal structure is initialized to have prescribed vertical and horizontal gradients. A reference point is chosen with some prescribed temperature, pressure, and composition, and from that point the compositions and pressures are calculated such that the vertical diffusive fluxes vanish, as described in more detail in a section addressing the numerical implementation. We now give details of the mathematical formulation.

2. Formulation

2.1. Diffusive Mass Flux and Darcy Flux Definitions

[10] We consider a system with n components (e.g., methane and ethane) and two possible fluid phases (liquid and vapor) in a potentially heterogeneous porous medium. Although the fluid phases can be separated at a "gas-oil contact" (GOC) at steady state because of the neglect of capillary pressure, there can also be both fluid phases present over an extended region during dynamic evolution. The mass diffusive flux of component i in phase α in the pores relative to the mass-averaged (barycentric) velocity of phase α in the pores is

$$\mathbf{j}_i^\alpha = \rho_i^\alpha (\mathbf{v}_i^\alpha - \mathbf{v}^\alpha) \tag{1}$$

Here $\mathbf{v}^\alpha$ is the barycentric velocity of phase α (mass averaged):

$$\mathbf{v}^\alpha = \sum_1^n (\omega_i^\alpha \mathbf{v}_i^\alpha). \tag{2}$$

$\mathbf{v}_i^\alpha$ is the velocity of component i in phase α and ω_i^α is the mass fraction of that component in phase α. In addition, ρ_i^α is the mass density of component i in phase α (kg of component i per m^3 of the phase). Here we use $\alpha = 1$ for the vapor (or gas) phase and $\alpha = 2$ for the liquid phase. The diffusion flux defined above has units of mass of component i (in kg) per area (in m^2) of the phase exposed on an area of the bulk surface per second. This makes the flux of mass of i per bulk area per time $\phi S^\alpha \mathbf{j}_i^\alpha$, where, ϕ is the porosity fraction and the phase saturation S^α varies between 0 and 1. Note that $S^{\alpha=1} = 1 - S^{\alpha=2}$.

[11] The molar diffusive flux relative to the molar average velocity $\mathbf{v}^{\alpha *}$ is

$$\mathbf{J}_i^{\alpha *} = c_i^\alpha (\mathbf{v}_i^\alpha - \mathbf{v}^{\alpha *}), \tag{3}$$

where

$$\mathbf{v}^{\alpha *} = \sum_1^n (x_i^\alpha \mathbf{v}_i^\alpha) \tag{4}$$

and x_i^α is the mole fraction of component i in phase α and c_i^α is the concentration of component i in phase α (moles of component i per m^3 of the phase).

[12] We define the mass-averaged Darcy flux of phase α in terms of the mass-averaged velocity of each individual phase [cf., *Allen*, 1985]:

$$\mathbf{q}^\alpha = \phi S^\alpha \mathbf{v}^\alpha. \tag{5}$$

The mass-averaged linear pore velocity is taken to be the barycentric velocity $\mathbf{v}^\alpha$ of phase α and is used as the logical reference velocity because gravity (force per mass) is involved in the transport law.

2.2. Flow Law and Mass Conservation

[13] We assume that the Darcy velocity of phase α depends on Darcy's law for that phase:

$$\mathbf{q}^{\alpha} = -\frac{\mathbf{k}k_r^{\alpha}}{\mu^{\alpha}} \bullet (\nabla p^{\alpha} + \rho^{\alpha} g \hat{\mathbf{k}}) \tag{6}$$

for phases α =1, 2. $\mathbf{k}$ is the permeability tensor, k_r^{α} is the relative permeability for phase α (between 0 and 1) for which we have used linear dependence upon the phase saturation as $k_r^{\alpha} = S^{\alpha}$, $\hat{\mathbf{k}}$ is the vertical unit vector, p^{α} is the pressure in phase α, g is the gravitational acceleration, ρ^{α} is the phase density $\rho^{\alpha} = \sum_i^n \rho_i^{\alpha}$ and μ^{α} is the dynamic viscosity of phase α. Mass balance for component i in phase α is given by

$$\frac{\partial}{\partial t}\left[\phi M_i \sum_{\alpha=1}^{2}(S^{\alpha} c_i^{\alpha})\right] + \nabla \bullet \left[\sum_{\alpha=1}^{2} \phi S^{\alpha}(M_i c_i^{\alpha} \mathbf{v}^{\alpha} + \mathbf{j}_i^{\alpha})\right] - Q_i = 0 \tag{7}$$

for components $i = 1, ..., n$. Here M_i is the molecular weight (kg/mole), S^{α} is the phase saturation in the pores, t is time, Q_i is the injection rate of component i (in kg of the component per bulk volume in m^3 per second), and $\mathbf{j}_i^{\alpha}$ is the mass diffusive flux of component i in phase α relative to the mass-averaged velocity of that phase. We define c^{α} as the phase molar density in phase α so that $c_i^{\alpha} = c^{\alpha} x_i^{\alpha}$. The above form of the transport equation is similar to the multiphase porous media formulation of *Bielinski* [2007] and *Allen* [1985]. The total molar density is (in moles/(m^3 fluid))

$$c = \sum_{\alpha=1}^{2}(S^{\alpha} c^{\alpha}). \tag{8}$$

We define z_i (moles of i per moles of fluid: including both the vapor and liquid phases if present) as the overall composition of component i averaged over both fluid phases:

$$c z_i = \sum_{\alpha=1}^{2}(S^{\alpha} c^{\alpha} x_i^{\alpha}), \tag{9}$$

and the rate of change of component i can be written as (in moles of i/(m^3 bulk)/sec)

$$U_i = \frac{\partial}{\partial t}(\phi c z_i). \tag{10}$$

Once c is found at the new time step, partitioning between the liquid and vapor phases is found by a phase split and stability calculation as described in *Firoozabadi* [1999] and *Li and Firoozabadi* [2012a, 2012b].

2.3. Diffusion Fluxes and Tortuosity

[14] The mass diffusion flux in phase α in the pores with components $i = 1, n-1$ relative to mass average pore velocity of phase α is

$$\mathbf{j}_i^{\alpha} = -\rho^{\alpha} \bar{\mathbf{T}}^{*} \left[\sum_{k=1}^{n-1}\left(D_{ik}^{M\alpha} \bullet \nabla \omega_k^{\alpha}\right) + D_i^{T\alpha} \bullet \nabla T + D_i^{P\alpha} \bullet \nabla p^{\alpha}\right], \tag{11}$$

where the tortuosity ($0 \le \bar{\mathbf{T}}^{*} \le 1$) [cf. *Bear*, 1972] can be anisotropic and heterogeneous. The placement of the tortuosity factor is consistent with *Bielinski* [2007] [see also *Ghorayeb and Firoozabadi*, 2000b]. See *Allen* [1985] for a discussion of hydrodynamic dispersion, which is normally neglected for low flow rates. In the above, $D_{ik}^{M\alpha}$, $D_i^{T\alpha}$, and $D_i^{P\alpha}$ are the molecular diffusion coefficients, the thermal diffusion coefficients, and the pressure diffusion coefficients, respectively [cf. *Firoozabadi et al.*, 2000], for a barycentric frame of a homogeneous fluid for the appropriate phases and components. We assume that the fluid pressures in each of the two phases are identical ($p^{\text{liq}} = p^{\text{vap}}$, as the capillary pressure is neglected). Also, the molar diffusion flux relative to the molar-averaged frame for $i = 1, n-1$ can be written as

$$\mathbf{J}_i^{\alpha *} = -c^{\alpha} \bar{\mathbf{T}}^{*} \left[\sum_{k=1}^{n-1}\left(D_{ik}^{M\alpha *} \bullet \nabla x_k^{\alpha}\right) + D_i^{T\alpha *} \bullet \nabla T + D_i^{P\alpha *} \bullet \nabla p^{\alpha}\right], \tag{12}$$

where the * on the Ds refers to the molar-averaged frame for the flux and the diffusion coefficients, which differ from the values in the mass-averaged frame [see also *Leahy-Dios and Firoozabadi*, 2007]. Calculations should be performed consistently (using D or D^{*}). Using mass-averaged velocities in the Darcy law formulation, it is most convenient to transform the molar fluxes in the molar frame into mass fluxes in the mass-averaged frame (for each phase separately) using the expression

$$\mathbf{j}_i^{\alpha} = \sum_{k=1}^{n-1}\left[\delta_{ik} + \left(\omega_n^{\alpha}(x_k^{\alpha}/x_n^{\alpha}) - \omega_k^{\alpha}\right)\frac{\omega_i^{\alpha}}{\omega_k^{\alpha}}\right] M_k \mathbf{J}_k^{\alpha *}, \tag{13}$$

where the indices i and k run from 1 to $n-1$ [cf. *de Groot and Mazur*, 1984, p. 243] and α = 1 or 2 (the phases). δ_{ik} is 1 for $i = k$ and 0 otherwise. The last component (n) may be calculated from

$$\mathbf{j}_n^{\alpha} = -\sum_{i=1}^{n-1} \mathbf{j}_i^{\alpha}, \tag{14}$$

but note that

$$\sum_{i=1}^{n} \mathbf{J}_i^{\alpha} \neq 0, \tag{15}$$

where $\mathbf{J}_i^{\alpha}$ is the molar flux in the mass-averaged frame, while the molar flux in the molar frame obeys

$$\sum_{i=1}^{n} \mathbf{J}^{*}{}_i^{\alpha} = 0, \tag{16}$$

and the mass-averaged flux in the mass-averaged frame obeys

$$\sum_{i=1}^{n} \mathbf{j}_i^{\alpha} = 0 \tag{17}$$

[cf. *de Groot and Mazur*, 1984, equation 30, p. 241]. The diffusion coefficients are further defined relative to the phenomenological coefficients in terms of fugacities, partial molar volumes, etc., [*Ghorayeb and Firoozabadi*, 2000c; *Firoozabadi et al.*, 2000].

2.4. Pressure Evolution

[15] The following equation may be solved for the evolution of pressure in the two-dimensional domain:

$$\frac{d\phi}{dp}\frac{\partial p}{\partial t} + \phi C_T \frac{\partial p}{\partial t} - \sum_{i=1}^{n} \bar{V}_{Ti} U_i = 0, \tag{18}$$

as discussed in *Acs et al.* [1985] and *Watts* [1986]. Our solution to the pressure equation is based on the

Table 1. Parameters Related to Thermal Evolution[a]

Thermal Conductivity λ (W/m/K)			Specific Heat $\hat{c}_p$ (J/kg/K)		Density ρ (kg/m^3)
Gas	Liquid	Solid	Fluid	Solid	Solid
0.035	0.10	3	2000	800	2650

[a]For the specific heat of the fluid, the parameter is $\hat{c}_p^*$ [cf. *Firoozabadi*, 1999, p. 183]; a single representative value for the mixture was used (based on *Passut and Danner* [1972]).

implicit approach. U_i includes source and sink terms (cf. equations (7) and (10)). In the above,

$$\bar{V}_{Ti} = \frac{\partial V_f}{\partial N_i}, \tag{19}$$

where N_i is the total number of moles of i in the vapor and liquid phases, and V_f is the total fluid volume in a reference volume. The two-phase isothermal compressibility of the fluid system is given by

$$C_T = -\frac{1}{V_f}\left(\frac{\partial V_f}{\partial p}\right). \tag{20}$$

2.5. Temperature Evolution

[16] Thermal evolution is derived from an energy equation. The dominant terms for two-phase flows in porous media are

$$\left[(1-\phi)\rho_s \hat{c}_{p:s} + \sum_{\alpha=1}^{2} \phi S^\alpha \rho_f^\alpha \hat{c}_{p:f}^\alpha\right](\partial T/\partial t) = \sum_{\alpha=1}^{2} \phi S^\alpha \left[\nabla \bullet (\lambda_f^\alpha \nabla T)\right] + (1-\phi)\left[\nabla \bullet (\lambda_s \nabla T)\right] - \sum_{\alpha=1}^{2} \phi S^\alpha \rho_f^\alpha \left(\hat{c}_{p:f}^\alpha \mathbf{v}^\alpha \bullet \nabla T\right). \tag{21}$$

Here the $\hat{c}_p$ represent the specific heat (by mass) for the indicated phase (solid, liquid, or vapor). We chose the reference ideal specific heats ($\hat{c}_{p:f}^*$) of the fluid from representative values in *Passut and Danner* [1972]. To find the values of $\hat{c}_{p:f}$ for use in the thermal evolution equation, we use the reference value. Because of the "per mass" definition of the specific heats, there is not much difference between the specific heats of the liquid and vapor phases at the conditions of our examples. The densities of the solid and relevant fluid phases are ρ_s and ρ_f^α. The thermal conductivities are similarly λ_s and λ_f^α. Values relevant to the thermal evolution are listed in Table 1.

2.6. Boundary Conditions and Governing Parameters

[17] For the simulations, the temperature distribution is either held fixed in time or is allowed to evolve by advection of heat. All examples presented had initial conditions with imposed horizontal and vertical temperature gradients.

[18] For the cases with evolving temperature in the domain, the temperatures at the upper and lower boundaries are held fixed as initialized, while vanishing lateral heat flux conditions are used at the vertical left and right side boundaries. The thermal conditions do not allow a static fluid because horizontal thermal gradients induce fluid motion.

[19] Part of our focus is on the similarities and differences that can evolve from differences in the initial conditions. To this end, we start the "convection-free initialization" (CFI) and then compute the domain averages for each of the components. In the "constant composition" initialization (CCI) cases that are compared to CFI, these average compositions are initially imposed throughout the domain.

[20] Other parameter values under consideration in modeling runs are as follows. Not all parameters can be practically varied due to the large number of possibilities. We considered several initial horizontal temperature gradients: 1.5, 3, and 6°C/km, T increasing to the right. The vertical temperature gradient is normally 20°C/km, T increasing downward. We present results for a ternary mixture of C_1 (methane), C_{10} (decane), and C_{20} (icosane); as well as an 11-component mixture representing a realistic reservoir fluid.

[21] A reference pressure is usually set at 500 m from the left-side boundary (x = 500) and z = 500 m up from the bottom (often near the middle of the depth) in the domain. Reference pressure is usually 600 bar. The reference temperature, chosen at the same reference point, is typically 400 K (kelvin). The domain size is generally 1 km deep and 2 km wide, with some other cases considered, e.g., 2 km deep or 10 km wide. We considered a wide range of permeabilities between 0.01 and 10,000 millidarcy but show only a small sampling of the results for the sake of brevity. The number of horizontal and vertical grid points were both 51. A

Table 2. Case Parameters[a]

Figure Example	Final Time (years)	Permeability (mdarcy)	Initialization	T_{ref} (K)	p_{ref} (bars)	N_x grid	N_z grid	L_x (km)	L_z (km)	$\partial T/\partial x$ K/km	Components
1	4 million	0.01	CCI, CCF	400	600	51	51	2	1	1.5	3
2	10 million	2000	CCI, CCF	400	600	51	51	2	1	1.5	3
3	200,000	500	CCI	400	600	51	51	2	2	1.5	11
4	5 and 20 million	0.1	CFI	404.26	445	51	51	10	1	1.5	11

[a]Here we show some of the parameters used in the simulations. The first column refers to the Figure number and the Example number. Default unless noted: $\partial T/\partial z$ = –20 K/km, Porosity fraction = 0.2, Reference point: fixed pressure at (x, z) = (500, 500) m (except for Example 4, where the reference point is at (x, z) = (500, 5000)m). N_x and N_z represent the number of grid points in the horizontal and vertical directions, respectively. L_x and L_z represent the domain extent in the horizontal and vertical directions. The constant composition initialization (CCI) and the "convection-free initialization" (CFI) are both listed if the Example compares these initializations. $\partial T/\partial x$ is the horizontal temperature gradient imposed as an initial condition. The figure numbers here are the same as the Example numbers.

Table 3a. Default Fluid Parameters for Ternary System: Compositions for Ternary Mixtures[a]

	Mole Fractions	
Number of Component: Carbons	CCI	CFI
z_1: C_1	0.3336788829689	0.333333
z_2: C_{10}	0.3328526503887	0.333333
z_3: C_{20}	0.3334684666423	0.333333

[a]Used in simulations with results shown in Figures 1 and 2 for Examples 1 and 2. For CCI, the compositions (initially constant throughout the domain) matched the CFI average composition of the whole domain (thereafter, compositions evolved by advective effects for both initializations). For the CFI case, the value listed is the composition at the reference point. The CFI initialization fills the domain with varying composition such that the pressure, temperature, and composition influences in the domain imply vanishing mass flux initially.

comparison to a higher-resolution run was made and is discussed below in Example 3.

[22] We will also show one example with modest rates of fluid injection and extraction at two different locations in a low-permeability domain. We used the tortuosity fixed as $\bar{\mathbf{T}}^* = 1$. See also the Tables 1–4.

2.7. Numerical Implementation

[23] The governing equations are solved by the finite volume method. At cell centers we define pressure, temperature, and composition. At cell edges we define velocities, diffusive fluxes, diffusion coefficients, permeability, relative permeability, viscosity, and tortuosity. A sparse matrix solver from UMFPACK is used for the solution of the pressure equation. The component evolution is calculated explicitly.

[24] For computations, the mass fluxes in the mass-averaged frame are converted back into molar fluxes in the mass-averaged frame by $\mathbf{J}_i^\alpha = \mathbf{j}_i^\alpha / M_i$, all in the mass-averaged frame for use in the calculation of mass conservation part of the code that had been previously written in terms of the molar fluxes. Each cell in the two-dimensional domain has sides defined by U, D, L, R (up, down, left, and right). In order for diffusion fluxes through a cell side to exist between cells for a particular phase, we assume that the phase in question must exist in both cells bounded by the side in question (otherwise, diffusion flux between cells does not occur for that phase in our formulation).

[25] As mentioned, for some cases the temperatures were held fixed. For other cases, after initial conditions were imposed, the domain interior allowed full thermal evolution as dictated by advection and diffusion of heat, while the temperatures are held to the initial values at the top and bottom boundaries, and the temperatures of the left and right boundaries are allowed to vary with the restriction that the normal (lateral) thermal fluxes vanish at those vertical boundaries. For locally constant thermal properties of the solid and fluid this is equivalent to $(\partial T/\partial x) = 0$ at the left and right vertical boundaries. These conditions are implemented through the use of fictitious points outside the domain so that the coded partial differential equations can have a uniform form throughout the domain. It should be mentioned that the time independence of the upper and lower boundary temperatures is imposed on one row of grid points outside the domains that we show for evolution of T (e.g., the lower boundary is not fixed within the computational domain, but it communicates with a layer of fictitious grid points just below the lower boundary that are held with time-independent temperatures).

[26] As mentioned above, the "constant composition" initialization (CCI) cases used average compositions of the domain from a comparable CFI case described below. The average compositions and constant pressure were initialized throughout the domain. Thermal conditions were initialized as described above. After initialization, there is a transient phase where the pressure adjusts to be nearly hydrostatic.

[27] The other choice for initial fluid composition is to solve for the composition that would have diffusion fluxes vanish in the vertical direction. This is called the "convection-free initialization" (CFI) [*Nasrabadi et al.*, 2006].

[28] For the "convection-free initialization" (CFI) compositions and pressures are calculated such that the vertical diffusive fluxes vanish. The thermal structure is initialized to have prescribed vertical and horizontal gradients. A reference point is chosen with some prescribed temperature, pressure, and composition, and from that point the compositions and pressures are calculated moving up and down from that point such that the pressure is hydrostatic, and the sum of the diffusive mass fluxes (due to gradients in composition, pressure, and temperature) vanish. For a two-dimensional domain, the composition across the bottom of the domain is calculated such that the sum of the horizontal diffusive fluxes vanish, while the pressure is matched to the horizontal neighbor. Once composition and pressure at the bottom

Table 3b. Default Fluid Parameters for Ternary System: Fluid Component Properties for the Ternary Mixture[a]

Component: Number of Carbons	T_c (K)	p_c (bar)	Acentric Factor	Mw (g/mole)	Critical Vol. (m^3/kg)	Shift Parm.	Molar Vol. (cm^3/mole)
z_1: C_1	190.56	45.99	0.011	16.04	0.00615	–0.154	32.407
z_2: C_{10}	617.07	21.55	0.534	142.00	0.00439	0.085	195.0
z_3: C_{20}	773.18	11.07	0.707	282.00	0.00420	0.193	350.0

[a]Used in simulations with results shown in Figures 1 and 2 for Examples 1 and 2. The τ parameter of the thermal diffusion coefficient (ratio of energy of vaporization to energy of viscous flow) for each component (dimensionless) is set to 4 [cf. *Shukla and Firoozabadi*, 1998]. Besides the compositions of each component, we also list the parameters used in the multicomponent phase behavior calculations [cf. *Firoozabadi*, 1999; *Hoteit et al.*, 2006] for the pure components: the critical temperature, the critical pressure, the asentric factor, the molecular weight, the critical volume, the shift parameters for volume translation (dimensionless), and the molar volumes of pure component at normal boiling point (cm^3/mole). Vapor and liquid phase viscosities for calculation of flow velocities were drawn from correlations, including *Lohrenz et al.* [1964].

Table 3c. Default Fluid Parameters for Ternary System: Binary Interaction Parameters [cf. *Hoteit et al.*, 2006][a]

Index	1	2	3
1	0	0.052	0.075
2	0.052	0	0
3	0.075	0	0

[a]Used in simulations with results shown in Figures 1 and 2 for Examples 1 and 2. The index refers to the component number.

of the domain have been calculated, one can calculate compositions and pressures moving up from each location (grid cell) along the bottom, while adjusting the composition to assure vanishing of the vertical diffusive mass fluxes and pressures that are hydrostatic. After initialization, some horizontal flows ensue because the horizontal pressure gradients may not be in balance with horizontal gradients in density. This initialization is often highly stratified, with lower molecular weight components concentrated near the top and heavier components favored near the bottom.

3. Discussion of the Results

[29] Temperatures are initialized in the domain via imposed horizontal and vertical gradients for the initial conditions (($\partial T/\partial x$) = constant and ($\partial T/\partial z$) = constant). We will discuss several cases that have been simulated. Cases for which we present figures are dubbed "Examples." We also summarize results of cases for which; for the sake of brevity, we do not include figures (these are given case letters for reference). Most of our results are for a ternary mixture of C_1 (methane), C_{10} (decane), and C_{20} (icosane) that allow full evolution of the thermal field by advection of heat, and this includes Examples 1 and 2. For Example 3, we allow full thermal evolution in an 11-component mixture representing a realistic reservoir fluid. In Example 4, we consider an 11-component mixture with fixed horizontal and vertical temperature gradients everywhere in the domain. This case also includes injection and extraction of fluid to represent seepage inflow and leakage.

3.1. Ternary Systems With Evolving Temperature

3.1.1. Case A: Comparison of Reference Frames With Evolving Temperature

[30] We compared the use of two different velocity frames of reference for a ternary fluid mixture via many simulations. The frames considered were the barycentric velocity frame of reference and the molar diffusive flux relative to the molar average velocity. The molar average velocity frame was used in *Nasrabadi et al.* [2006, 2007] and *Ghorayeb and Firoozabadi* [2000b]. With gravity involved, the proper choice is the barycentric velocity frame of reference. In fact, in our simulations there were only small difference between the results, with the difference typically in the ninth significant figure for the mole fractions. We would anticipate larger differences between results using the two different frames for cases of larger fluid velocities or fluids closer to the critical point. These comparisons lend confidence to prior results that used the molar average reference frame. The ternary we consider is composed of methane, decane, and icosane (C_1, C_{10}, and C_{20}, with the number of carbons indicated). We ran simulations for up to 2 Ma using many different permeabilities between 0.01 mdarcy and 2 darcies, and most cases were initialized with constant composition (CCI). The pressure was held fixed at the reference point. The initial T and p values at the reference point were the same as those used for Examples 1 and 2.

3.1.2. Example 1: Comparison of CCI and CFI Initializations for Low Permeability With Evolving Temperature

[31] For Example 1, with results shown in Figure 1, we compared two cases, one is initialized with the constant composition initialization (CCI) and the other with the "convection-free initialization" (CFI), both for a permeability of 0.01 mdarcy. The pressure is held fixed at the reference point. The simulation is run for 4 Ma, at which time the CCI case is nearly at steady state and the CFI case is not quite steady. The barycentric velocity frame of reference is used for both cases. In fact, there is little difference between the results. In the Figure 1, we show only the CCI case. For temperature, pressure, and density, the largest percent differences for the maximum (or minimum) values between the CCI and CFI cases at the end of the simulations were less than 4×10^{-4}%. The maximum percent difference (calculated in a similar way) for z_1, z_2, and z_3, were respectively 6×10^{-3}%, 0.02%, and 0.02%. The CCI case evolves toward the typical CFI case, with C_1 (z_1) and C_{20} (z_3) showing expected stratification (light on the top and heavy on the bottom). The C_{10} component (z_2) is more complicated, tending to concentrate in the upper left (relatively cool and low pressure) part of the domain and of low values on the lower right (warm and higher pressure). The velocities are a bit different for the CCI and CFI cases. For the CCI case, there is some influence of the fact that the pressure is held fixed at the reference point at $x = z = 500$ m, which appears to be providing a slight suction (flow into the reference point) at

Table 4a. The 11-Component Fluid Parameters: Fluid Compositions for Examples 3 and 4[a]

Component #	Carbon or Fraction #	Initial Mole Fraction	Injection (Ex. 4) Mole Fraction
1	C_1	0.59038	0.60038224
2	C_2	0.08490	0.07489738
3	C_3	0.04150	0.03149880
4	nC_4	0.03090	0.02089910
5	nC_5	0.01970	0.00969940
6	C_6	0.01750	0.01749950
7	F_1	0.03420	0.03419900
8	F_2	0.06209	0.06209209
9	F_3	0.06127	0.06126819
10	F_4	0.04039	0.04038880
11	F_5	0.01718	0.04717550

[a]Used for Examples 3 and 4. The τ (dimensionless) for each component is set to 4 (cf. Table 3 for this and other parameter definitions). For Example 3, $k_v/k_h = 1$ (the permeabilities in the vertical and horizontal directions). Pressure and compositions were allowed to float at reference point. For Example 4, we used anisotropic permeability $k_v/k_h = 0.1$ (all other cases had this ratio as 1) with k_h=0.1 mdarcy. Injection started 100,000 years into the simulation and ramped up to the full injection rate (50 kg/yr) by 200,000 years. Final time= 20 million years. At the reference point at $(x, z) = (500, 5000)$ m, the pressure was held fixed, but the composition was allowed to float (composition changed naturally with input of fluid entering the extraction point). Examples 3 and 4 fluid properties are C for standard component, F for fractions, defined by fluid properties in Table 4b. For Example 4, injection point is at $x = 490.196$ m, $z = 49.019$, the index (3,3) grid location.

Table 4b. The 11-Component Fluid Parameters: Fluid Properties for the Components of the Mixture Used in Examples 3 and 4

Component #	T_c (K)	p_c (bar)	Acentric Factor	Mw (g/mole)	Critical Vol. (m^3/kg)	Shift Parm.	Molar Vol. (cm^3/mole)
1	190.560	45.990	0.011	16.040	0.00615	–0.154	32.407
2	305.320	48.720	0.099	30.070	0.00484	–0.100	48.347
3	369.830	42.480	0.153	44.100	0.00454	–0.085	66.722
4	425.120	37.960	0.199	58.120	0.00439	–0.064	85.264
5	469.700	33.700	0.251	72.150	0.00431	–0.042	105.106
6	507.400	30.120	0.296	86.180	0.00422	–0.002	125.049
7	564.300	29.992	0.295	99.590	0.00492	0.052	130.000
8	644.700	24.070	0.410	141.430	0.00617	0.081	200.000
9	748.300	17.313	0.617	220.870	0.00439	0.135	380.000
10	852.800	12.286	0.905	347.850	0.00492	0.175	430.000
11	955.200	9.101	1.258	550.000	0.00617	0.163	670.000

this point in the simulation. Some fluid exchange at the reference point can occur to maintain the fixed reference pressure. Maximum vertical (mass-averaged) Darcy velocities (absolute values) are on the order of 1.4×10^{-6} m/yr for the CCI case and about half that for the CFI case, but away from the constant pressure reference point, the velocities are almost the same for the two cases. This striking similarity between these two cases will be contrasted below (Example 2) for a case where the different initializations lead to very different end states. The weak flow has an upwelling (fluid going upward) at the right boundary and a downwelling (fluid going downward) on the left side. See Tables 2 and 3 for other details. The pressure is nearly hydrostatic for all cases we examined, except for the case with injection (Example 4). The thermal structure is typically dramatically modified from the initial conditions (imposed thermal gradients in the x and z directions), if the fluid velocities are strong enough to cause significant advection of heat.

3.1.3. Case B: Comparison of Initializations for 100 mdarcy With Evolving Temperature

[32] We compared two cases, one using the "constant composition initialization" and the other using the "convection-free initialization" for a permeability of 100 mdarcy. The simulation was run for 2 Ma, with other parameters as used for Example 1. Although the CCI and CFI cases were not quite at steady state, there was little difference between the results. The CCI case showed significant unmixing, but with the compositions tending toward those of the CFI case. The fluid velocities were small, with fluid that upwelled on the left and right and a single downwelling in the near the center (of slightly different locations for the two cases).

3.1.4. Case C: Comparison of Initializations for 500 mdarcy With Evolving Temperature

[33] We also compared the CCI and CFI initializations for a permeability of 500 mdarcy. The simulations were run for 2 Ma, with other parameters as used for Example 1. Both the CCI and CFI cases were not quite at steady state. There was a dramatic difference between these cases. For CCI, there was modest unmixing, with the methane composition nearly uniform on the left side, but with significant gradients toward low values at the lower right of the domain. The C_{20} component was similar to C_1, but with the opposite trends. Both cases had a downwelling on the left side and an upwelling more or less at the center of the domain, but the CFI case had velocities about 17 times less than the CCI case.

3.1.5. Example 2: Comparison of Initialization for 2 Darcies With Evolving Temperature

[34] This example is notable because two different initial conditions with the same initial thermal conditions and essentially the same average composition seem to evolve to very different steady states. For Example 2, with results shown in Figure 2, we compare the CCI and CFI initializations, for a permeability of 2 darcies. The constant composition initialization (CCI) results are placed above the "convection-free initialization" (CFI) results. The simulation is run for 10 Ma; at which time, the CCI case is at steady state, and the CFI case is almost steady. For the CCI case, the fluid remains with nearly constant composition, being mixed by the fluid flow. There is some slight unmixing that is consistent with the thermal gradients and the diffusion coefficients of the components (which diffuse due to gradients in p, T, and composition). The CFI case results in a distribution of fluid components that are gravitationally segregated for z_1 and z_3, but not for z_2, and has very small fluid velocities. The CCI case exhibits two upwellings and two downwellings and a significant and steady perturbation of the thermal field compared to the CFI case. Remarkably, the simulations achieve nearly steady states with very different distributions of temperature and composition for the two different initial conditions, even though the average fluid compositions are essentially the same. This should not be too surprising for the evolution of nonlinear systems. One case (CCI) advects heat with significant motion, with noticeable changes in the final thermal structure. The other case (CFI) remains gravitationally segregated because the hydrostatic and compositionally segregated convection-free initialization inhibits vertical motion. The CCI lacks the compositional segregation that could inhibit significant vertical motion.

Table 4c. The 11-Component Fluid Parameters: Binary Interaction Parameters Used in Examples 3 and 4[a]

$I_{1,1}$	$I_{1,2}$	$I_{1,3}$	$I_{1,4}$	$I_{1,5}$	$I_{1,6}$	$I_{1,7}$	$I_{1,8}$	$I_{1,9}$	$I_{1,10}$	$I_{1,11}$
0	0	0	0	0	0	0.037	0.028	0.038	0.146	0.125

[a]Note that $I_{1,j}=I_{j,1}$ and that for this case all other $I_{i,j} = 0$.

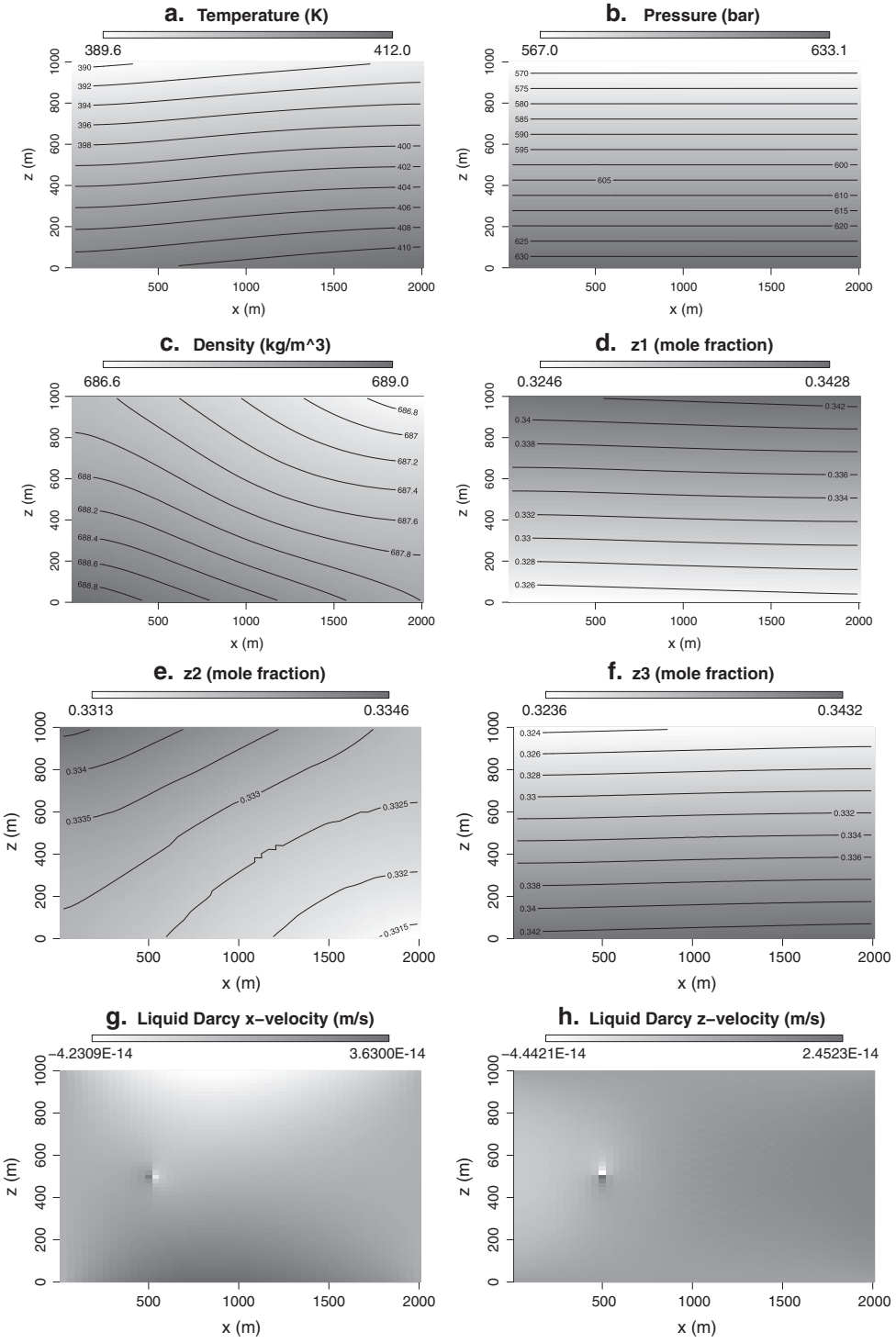

Figure 1. Example 1: The constant composition initialization (CCI) for a permeability of 0.01 mdarcy after 4 Ma. We also ran the "convection-free initialization" (CFI) (not shown, but very similar, see text). See Tables 2 and 3 for other details. (a) Temperatures in the *x*-*z* domain, (b) pressure, (c) fluid density, (d) mole fraction of z_1 (methane, C_1), (e) mole fraction of z_2 (C_{10}), (f) mole fraction of z_3 (C_{20}), (g) horizontal component of the Darcy velocity, and (h) the vertical component of the Darcy velocity.

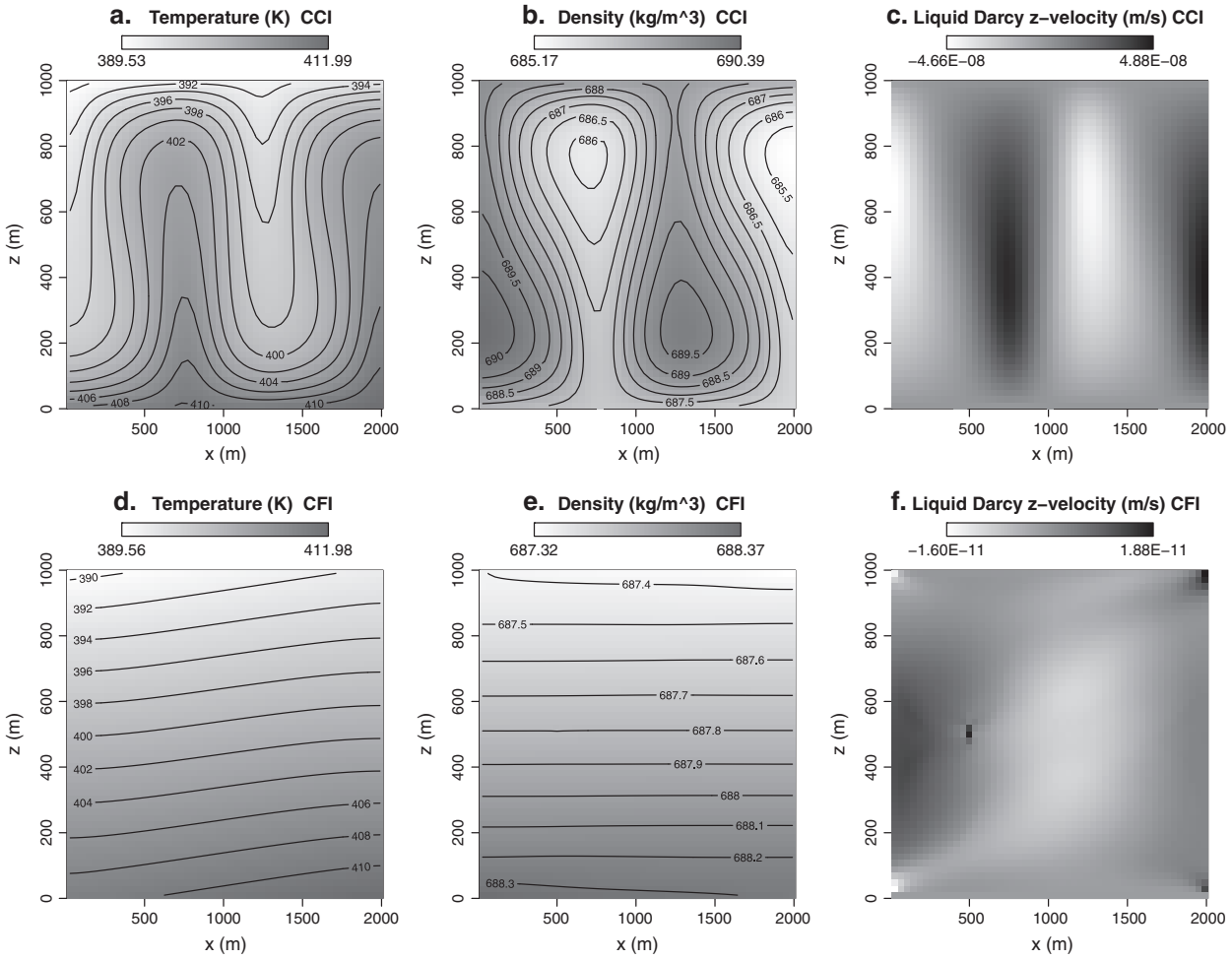

Figure 2. Example 2: Comparison of the constant composition initialization (CCI) (on the top in each figure part) and the "convection-free initialization" (CFI) (always on the bottom) for a permeability of 2 darcy. The simulation is run for 10 Ma. (a) Temperature, (b) fluid density, and (c) the vertical velocity, all for the CCI case. (d) Temperature, (e) fluid density, and (f) the vertical velocity (about 3 orders of magnitude smaller than the CCI case), all for the CFI case. (g) z_1 (methane, C_1), (h) z_2 (C_{10}), (i) z_3 (C_{20}), all for the CCI case. (j) z_1 (methane), (k) z_2 (C_{10}), (l) z_3 (C_{20}), all for the CFI case.

3.1.6. Case D: Initialization Comparison for Larger Horizontal Temperature Gradients and Evolving Temperature

[35] We compared the CCI and CFI initializations for a permeability of 2 darcies but with a larger horizontal thermal gradient. We examined the influence of increasing the horizontal thermal gradient to 3 K/km (previous cases used 1.5 K/km) of the initial conditions. The simulations were run for 2 Ma, and both cases achieved steady states. The CCI case exhibited a single upwelling on the right and a downwelling at the left, while the CFI case had upwellings at both side boundaries and a single downwelling centered around $x = 700$ m. Both cases had similar velocity magnitudes on the order of 1 m/yr. The thermal field of each case was strongly influenced by convection. The CCI case had minor unmixing (compared to its initial values independent of position), with the development of boundary layers. What was remarkable, however, was that the CFI case became much more homogenized compared to its initial gravitationally segregated spatial distribution.

3.1.7. Case E: Initialization Comparison for Even Larger Horizontal Temperature Gradients and Evolving Temperature

[36] We examined the influence of further increasing the initial horizontal thermal gradient to 6 K/km. We again compared the CCI and CFI initializations for a permeability of 2 darcies. The simulation was for 2 Ma, but both cases achieved steady state in less than 100,000 years. The results of both cases were almost identical, with a single upwelling on the right side and a downwelling at the left of similar magnitudes. Both cases had significant thermal changes from the initial conditions due to advection of heat. The compositions were also nearly identical, with near-uniform composition and implies significant mixing from the CFI initial state and minor unmixing of the CCI initial state.

3.2. Mixture Evolution With the 11 Components

[37] We present two examples for evolving 11-component mixtures; one with evolving temperatures and one with a fixed temperature distribution.

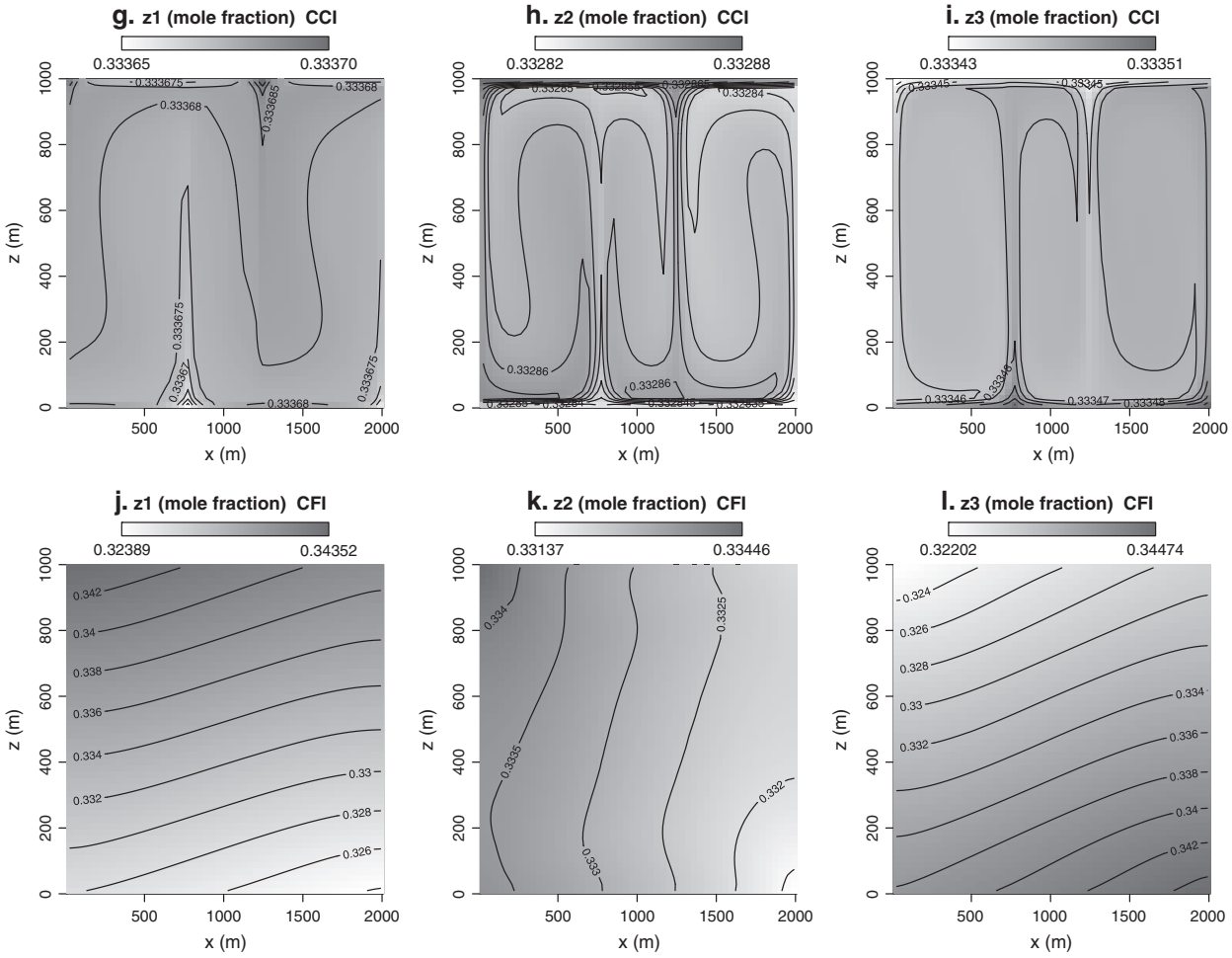

Figure 2. (continued)

3.2.1. Example 3: The 11-Component Mixture With Evolving Temperature

[38] We show results for Example 3 in Figure 3 for an example of an 11-component fluid (instead of the ternary fluid mixtures described above). We chose a larger layer depth and a permeability of 500 mdarcy. The domain is 2 by 2 km in x and z. We use CCI and allow the reference point to freely evolve T, p, and composition. Steady state is achieved in about 30,000 years, but the simulation was run up to 200,000 years. The maximum magnitude of the vertical Darcy velocity is about 0.5 m/yr. One upwelling at the right and one downwelling at the left is observed. Given the characteristic Darcy velocity (and a 0.2 porosity fraction), the characteristic time for fluid to transit all the way around the edges of the domain (8 km) would be on the order of 3200 years. Thus, the steady state is achieved in $\sim$9.4 turnover times. The unmixing of the fluid components is slight, implying near-uniform composition. The most pronounced "unmixing" occurred along the upper and lower boundaries, where the thermal gradients are strongest. Some residual advected unmixed fluids exist in the upwelling plume on the right boundary and in the downwelling plume at the left boundary.

[39] Our simulations used 51 $\times$ 51 grid points used in the horizontal and vertical. We compared that resolution to about double the resolution (101 $\times$ 101 grid points). The resolution test compared these grids for the conditions of Example 3 at a time of 30,000 years (after the system was essentially at steady state). The qualitative results were the same. The magnitude of the fluid velocities for the higher-resolution run were about 2% larger than the low-resolution run. The maximum compositional difference was for z_{11} (1.7% difference), while all other compositions were less than 0.5% different. The fluid density differed by less than 0.05%.

3.2.2. Example 4: The 11-Component Mixture With Fixed Temperature Gradients Everywhere

[40] Example 4 is another case study for an 11-component mixture with results shown in Figure 4. This is the only case we present that has a distinct gas-oil contact. As noted, the thermal structure was fixed everywhere, independent of time. This simulation shows the dramatic effect of filling (seepage inflow) and leakage (seepage outflow) of fluids. We show results at 5 and 20 Ma into the simulation, with more details of the simulation in Table 4. Steady state is not quite achieved. The permeability is 0.1 mdarcy, and the injection rate is 50 kg/yr. Given that the simulation is two dimensional, this value should be interpreted as the quantity injected per meter in the direction into the plane of the figure, as if there were a line source in the y direction if the

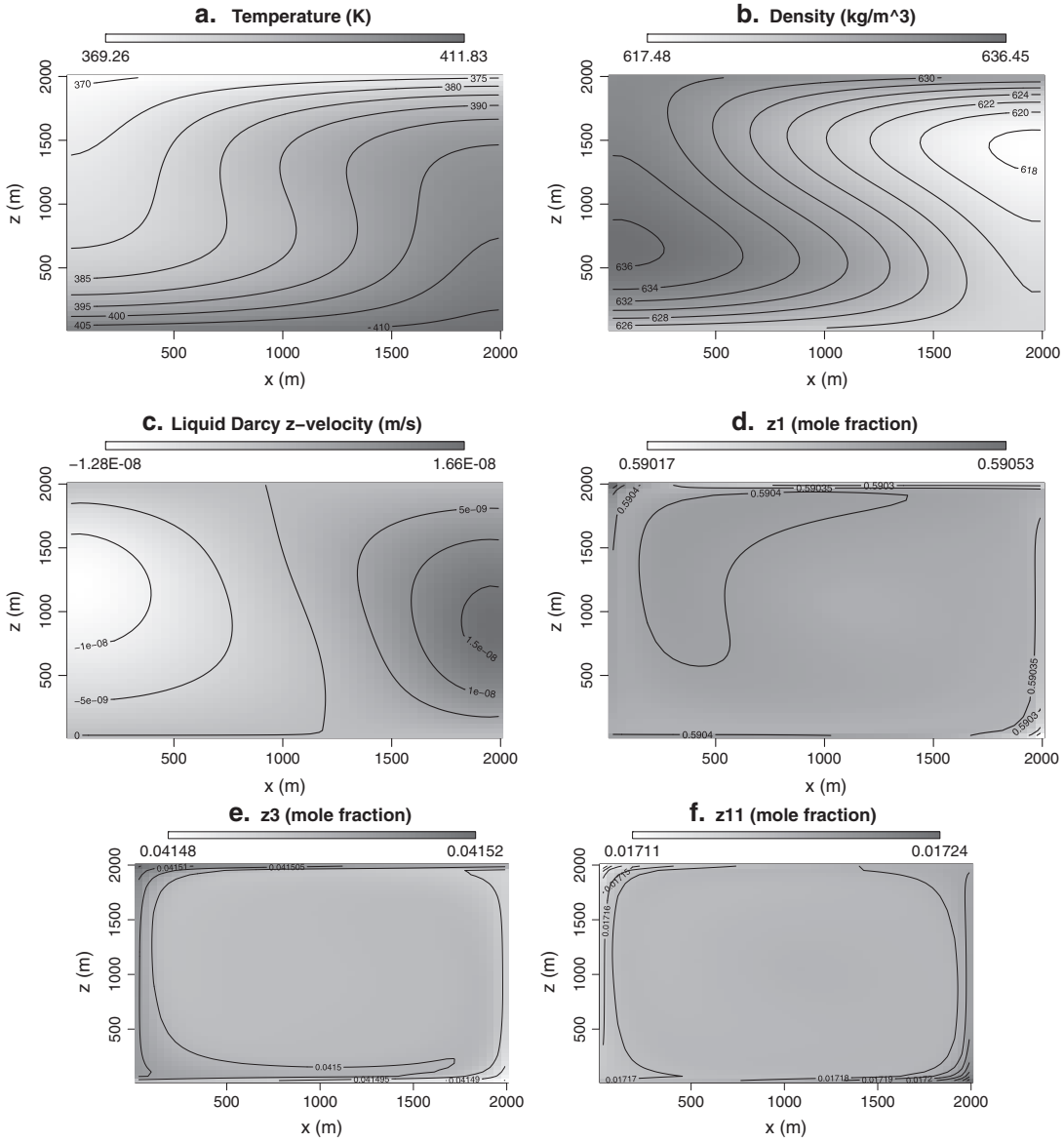

Figure 3. Example 3: A simulation with a larger layer depth (2 km) and 11 components using the constant composition initialization. The permeability is 500 mdarcy, and the simulation is run for 200,000 years. (a) Temperature, (b) fluid density, (c) the vertical velocity, (d) z_1 (methane). The rest of the figure parts show the other components: (e) z_3 and (f) z_{11}.

system were three dimensional. Fluid is allowed to seep out at the reference point in the center of the domain, at a rate determined by the fact that this point is held at the fixed pressure of 445 bar. At this extraction point, the composition was allowed to "float", i.e., to vary as new fluid entered the grid point where fluid left the system. Thermal evolution is suppressed, and the barycentric reference frame is used. This case has a distinct gas-oil contact (GOC) slightly above the center of the domain (vapor (gas) phase above the GOC and liquid phase below it). Relative to the initial composition of the reference point, the injected fluid is enriched in C_1 and the z_{11} (the 550 g/mole heaviest fraction), but depleted in C_2, C_3, C_4, and C_5 (cf. Table 4). Figure 4c shows the C_1 enrichment as a plume above the injection point. The GOC is displaced upward by the injection. Figures 4e and 4f show line segments for the liquid and vapor phase velocities, respectively. The long line segments near the central reference point just indicate that fluid is being extracted. Also shown are the horizontal Darcy velocities (in gray in Figure 4e) and the vertical velocities (in gray in Figure 4f) both in meters per second (or properly $m^3/m^2/s$), where we have summed the liquid and vapor phase velocities (almost all cells in the domain are either liquid or vapor, rather than a mixture of phases). Figures 4g–4n show some measures of the system after 20 Ma, at which time the GOC is further displaced. Fluid compositions on the right side of the domain and away from the extraction point are relatively isolated with compositions changing only a small amount, while between the injection and extraction points the compositions are much affected.

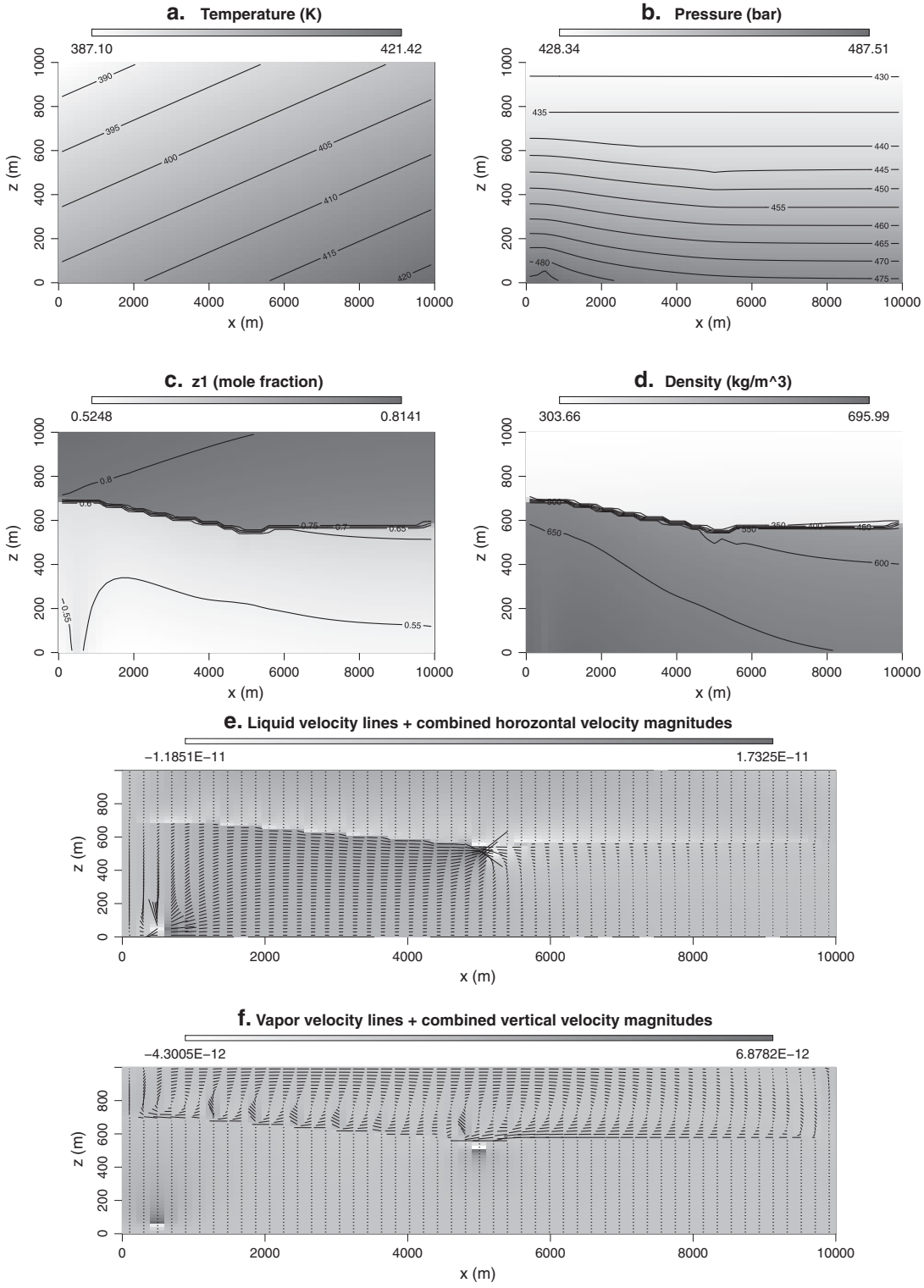

Figure 4. Example 4: A Simulation with injection and withdrawal of fluid and a GOC. The injection rate is 50 kg/yr, the permeability is 0.1 mdarcy. (a) temperature, (b) pressure, (c) z_1 (methane), (d) fluid density, (e) velocity line segments for the liquid, (f) velocity line segments for the vapor. Also shown are the horizontal Darcy velocities (in gray in Figure 4e) and the vertical velocities (in gray in Figure 4f) both in meters per second (or $m^3/m^2/s$), where we have summed the liquid and vapor phase velocities (almost all cells in the domain are either liquid or vapor, rather than a mixture of phases). Figures 4a–4f are all for 5 Ma into the simulation. The rest of the figure parts are after 20 Ma of simulation. (g) z_1 (methane), (h) pressure, (i) z_2 (ethane), (j) fluid density, (k) z_3 (propane), (l) z_5 (n-pentane), (m) z_6 (hexane), and (n) z_{11} (550 g/mole fraction).

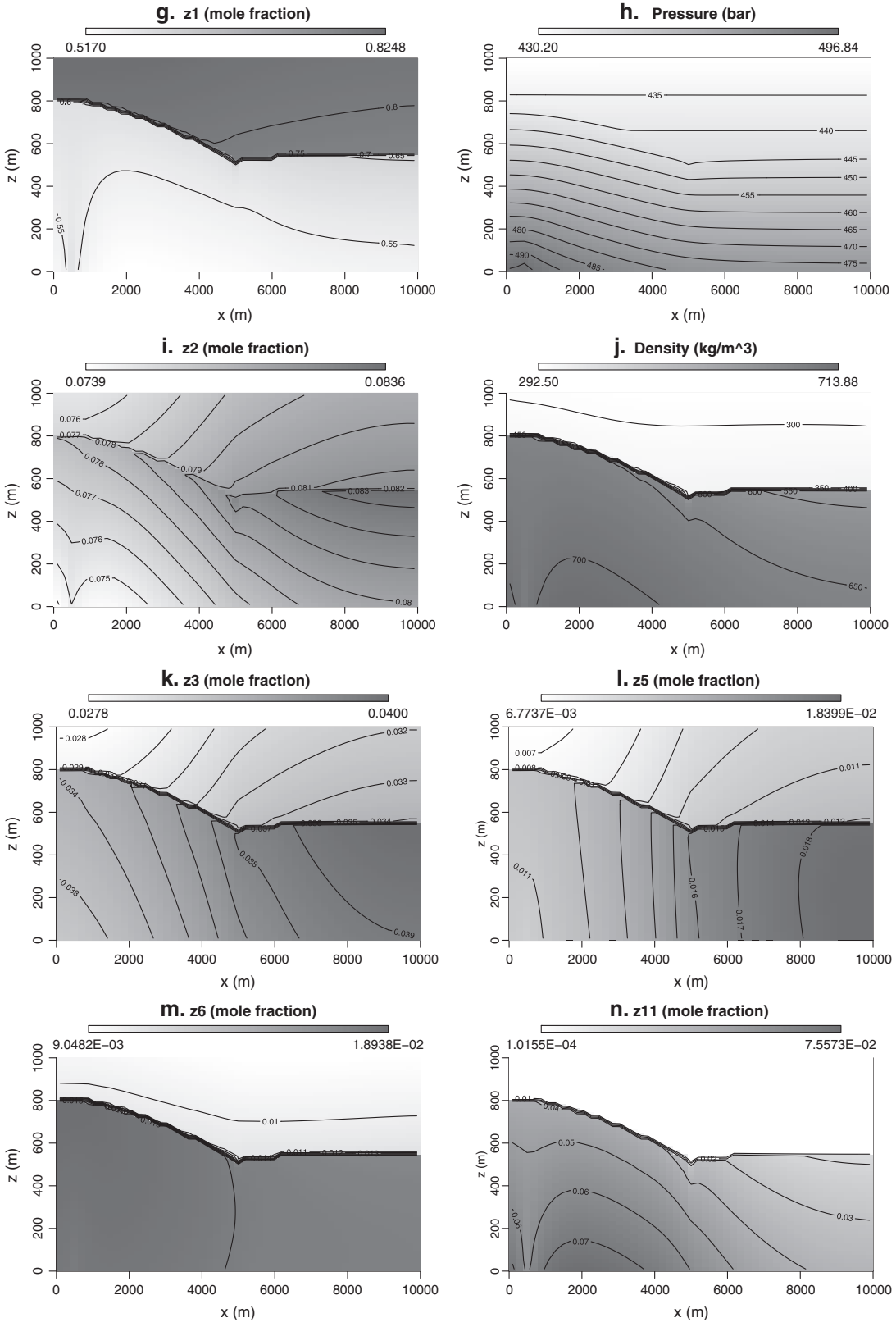

Figure 4. (continued)

4. Summary and Concluding Remarks

[41] We highlight some of the main results of this study:

[42] 1. Comparison of two different initial conditions (constant composition initialization CCI and the "convection-free initialization" CFI) shows that the system evolves to the same state for low permeabilities (stratified with significant compositional variation).

[43] 2. For high permeabilities, or strong horizontal thermal gradients, the initializations also end up with similar states (nearly uniform composition).

[44] 3. Some cases (e.g., those discussed in Example 2) can lead to two very different steady states, dependent on the initial conditions. It is not too surprising that nonlinear systems evolve with different time dependence, but what is interesting here is that the final independent states can be steady.

[45] Vigorous thermal convection can lead to nearly uniform reservoir composition. Slight unmixing of initially constant composition reservoirs is consistent with simultaneous diffusion via pressure, temperature, and compositional forcing as well as advective mixing.

[46] We have also performed many simulations with 1 km depth and a 10 km width. Many of these tend to exhibit multicellular convection with cell sizes similar to those shown here (the cell width being similar to the cell depth). Some of these wider systems seemed more prone to homogenization for the same permeability than what we have shown here. We cannot at this time be sure if that is due to insufficient numerical resolution of the large lateral extent systems. We have also done many simulations with 10 darcy permeability that not only showed nearly uniform composition but dramatic time dependence as well, with multiple and changeable upwelling and downwelling blobs typical of chaotic convection. Other cases of convection in binary hydrocarbon systems are discussed in *Riley and Firoozabadi* [1998].

[47] **Acknowledgments.** We thank H. Nasrabadi, W. Mutoru, and H. Hoteit for their useful discussions and help with various aspects of numerical codes. We also thank ExxonMobil for support of this project.

References

Acs, G., S. Doleschall, and E. Farkas (1985), General purpose compositional model, *Soc. Pet. Eng. J.*, *25*(4), 543–553.

Allen, M. B. III (1985), Numerical modelling of multiphase flow in porous media, *Adv. Water Res.*, *8*, 162–187.

Abbasi, A., M. Z. Saghir, and M. Kawaji (2011), Study of thermodiffusion of carbon dioxide in binary mixtures of n-butane & carbon dioxide and n-dodecane & carbon dioxide in porous media, *Int. J. Therm. Sci.*, *50*, 124–132.

Bear, J. (1972), *Dynamics of Fluids in Porous Media*, 784 pp., Elsevier, New York.

Bielinski, A. (2007), Numerical Simulation of CO_2 Sequestration in Geological Formations, PhD dissertation, Institut für Wasserbau der Universität Stuttgart. ISBN 3-933761-58-1, 117 p.

Bolton, E. W., A. C. Lasaga, and D. M. Rye (1996), A model for the kinetic control of quartz dissolution and precipitation in porous media flow with spatially variable permeability: Formulation and examples of thermal convection, *J. Geophys. Res.*, *101*, 22,157–22,187.

Bolton, E. W., A. C. Lasaga, and D. M. Rye (1999), Long-term flow/chemistry feedback in a porous medium with heterogeneous permeability: Kinetic control of dissolution and precipitation, *Am. J. Sci.*, *299*, 1–68.

Bories, S. A., and M. A. Combarnous (1973), Natural convection in a sloping porous layer, *J. Fluid Mech.*, *57*, 63–79.

Caltagirone, J. P. (1975), Thermoconvective instabilities in a horizontal porous layer, *J. Fluid Mech.*, *72*, 269–287.

Chapman, S. (1955), The molecular diffusive rate of change of composition in the atmosphere, *J. Meteorol.*, *12*, 111–116.

de Groot, S. R., and P. Mazur (1984), *Non-Equilibrium Thermodynamics*, 510 pp., Dover Publications, New York.

di Primio, R., and J. E. Skeie (2004), Development of a compositional kinetic model for hydrocarbon generation and phase equilibria modelling: A case study from Snorre Field, Norwegian North Sea, *Geol. Soc. London, Spec. Publ. 2004*, *237*, 157–174, doi:10.1144/GSL.SP.2004.237.01.10.

Firoozabadi, A. (1999), *Thermodynamics of Hydrocarbon Reservoirs*, 355 pp., McGraw Hill, New York.

Firoozabadi, A., K. Ghorayeb, and K. Shukla (2000), Theoretical model of thermal diffusion factors in multicomponent mixtures, *AlChE J.*, *46*(5), 892–900.

Ghorayeb, K., and A. Firoozabadi (2000a), Numerical study of natural convection and diffusion in fractured porous media, *SPE J.*, *5*(1), 12–20.

Ghorayeb, K., and A. Firoozabadi (2000b), Modeling multicomponent diffusion and convection in porous media, *SPE J.*, *5*(2), 158–171.

Ghorayeb, K., and A. Firoozabadi (2000c), Molecular, pressure, and thermal diffusion in nonideal multicomponent mixtures, *AlChE J.*, *46*(5), 883–891.

Ghorayeb, K., A. Firoozabadi, and T. Anraku (2003), Interpretation of the unusual fluid distribution in the Yufutsu gas-condensate field, *SPE J.*, *8*(2), 114–123.

Helgeson, H. C., L. Richard, W. F. McKenzie, D. L. Norton, and A. Schmitt (2009), A chemical and thermodynamic model of oil generation in hydrocarbon source rocks, *Geochim. Cosmochim. Acta*, *73*, 594–695.

Hoteit, H., E. Santiso, and A. Firoozabadi (2006), An efficient and robust algorithm for the calculation of gas-liquid critical point of multicomponent petroleum fluids, *Fluid Phase Equilib.*, *241*, 186–195.

Leahy-Dios, A., and A. Firoozabadi (2007), A unified model for nonideal multicomponent molecular diffusion coefficients, *AlChE J.*, *53*(11), 2032–2939.

Leythaeuser, D., and J. Rückheim (1989), Heterogeneity of oil composition within a reservoir as a reflection of accumulation history, *Geochim. Cosmochim. Acta*, *53*, 2119–2123.

Li, Z., and A. Firoozabadi (2012a), Initialization of phase fractions in RachfordRice equations for robust and efficient three-phase split calculation, *Fluid Phase Equilib.*, *332*, 21–27.

Li, Z., and A. Firoozabadi (2012b), General strategy for stability testing and phase-split calculation in two and three phases, *SPE J.*, *17*(4), 1096–1107.

Lohrenz, J., B. G. Bray, and C. R. Clark (1964), Calculating viscosities of reservoir fluids from their compositions, *J. Pet. Technol.*, *16*(10), 1171–1176.

Nasrabadi, H., K. Ghorayeb, and A. Firoozabadi (2006), Two-phase multicomponent diffusion and convection for reservoir initialization, *SPE Reservoir Eval. Eng.*, *9*(5), 530–542.

Nasrabadi, H., H. Hoteit, and A. Firoozabadi (2007), An analysis of species separation in a thermogravitational column filled with a porous medium, *Transp. Porous Media*, *67*, 473–486, doi:10.1007/s11242-006-9037-8.

Palm, E. (1990), Rayleigh convection, mass transport, and change in porosity in layers of sandstone, *J. Geophys. Res.*, *95*(B6), 8675–8679.

Passut, C. A., and R. P. Danner (1972), Correlation of ideal gas enthalpy, heat capacity, and entropy, *Ind. Eng. Chem. Process Des. Dev.*, *11*(4), 543–546.

Riley, M. F., and A. Firoozabadi (1998), Compositional variation in hydrocarbon reservoirs with natural convection and diffusion: Two-Component single-phase fluid, *AlChE J.*, *44*(2), 452–464.

Shukla, K., and A. Firoozabadi (1998), A new model of thermal diffusion coefficients in binary hydrocarbon mixtures, *Ind. Eng. Chem. Res.*, *37*(8), 3331–3342, doi:10.1021/ie970896p.

Watts, J. W. (1986), A compositional formulation of the pressure and saturation equations, *SPE Reservoir Eng.*, *1*(3), 243–252.

Wood, J. R., and T. A. Hewett (1982), Fluid convection and mass transfer in porous limestones: A theoretical model, *Geochim. Cosmochim. Acta*, *46*, 1707–1713.